ADVANCED MATERIALS INTERFACES
www.advmatinterfaces.de

Surface Modification of a MXene by an Aminosilane Coupling Agent

Hossein Riazi, Mark Anayee, Kanit Hantanasirisakul, Ahmad Arabi Shamsabadi, Babak Anasori, Yury Gogotsi, and Masoud Soroush*

MXenes, 2D transition metal carbides and/or nitrides, possess surface termination groups such as hydroxyl, oxygen, and fluorine, which are available for surface functionalization. Their surface chemistry is critical in many applications. This article reports amine functionalization of $Ti_3C_2T_x$ MXene surface with 3-(2-aminoethylamino)-propyltrimethoxysilane (AEAPTMS). Characterization techniques such as X-ray photoelectron spectroscopy verify the success of the surface functionalization and confirm that the silane coupling agent bonds to $Ti_3C_2T_x$ surface both physically and chemically. The functionalization changes the MXene surface charge from −35 to +25 mV at neutral pH, which allows for in situ preparation of self-assembled films. Further, surface charge measurements of the functionalized MXene at different pH show that the functionalized MXene has an isoelectric point at a pH around 10.7, and the highest reported surface charge of +62 mV at a pH of 2.58. Furthermore, the existence of a mixture of different orientations of AEAPTMS and the simultaneous presence of protonated and free amine groups on the surface of $Ti_3C_2T_x$ are demonstrated. The availability of free amine groups on the surface potentially permits the fabrication of crosslinked electrically conductive MXene/epoxy composites, dye adsorbents, high-performance membranes, and drug carriers. Surface modifications of this type are applicable to many other MXenes.

1. Introduction

MXenes are a large family of 2D transition metal carbides and/or nitrides derived primarily through the selective etching of the A-group element layers in layered ternary transition metal carbides and/or nitrides (MAX phases) with hydrofluoric acid (HF) or in situ generation of HF using lithium fluoride and hydrochloric acid.[1–3] The general formula of MAX is $M_{n+1}AX_n$ and that of MXene is $M_{n+1}X_nT_x$, where "M" is an early transition metal "A" is a group 13 or 14 element such as Al and Si, "X" is C and/or N, and "T" represents surface functional groups such as O, OH, F, and Cl.[4] The integer "n" is between 1 and 3. After etching, the multilayer MXene nanosheets can be delaminated into single-layer flakes by manual shaking or sonication.[5] $Ti_3C_2T_x$ was the first MXene discovered and remains the most widely studied MXene primarily due to the well-established methods for synthesis and material handling.[6] The negative surface charge of −39.4 mV is reported for fresh $Ti_3C_2T_x$ which originates from the negatively charged surface terminations.[7] MXenes retain their negative surface charge in the wide pH range of 4–12, resulting in high colloidal stability that enables facile solution processing and surface modifications.[8] Similar to other 2D nanomaterials, MXenes usually appear in the form of stacked sheets and their properties strongly depend on their morphology—stacked bundles versus individual sheets—and the type of chemical species present between the 2D flakes and on the surface.[9,10]

Silane coupling agents are capable of forming durable bonds between organic and inorganic materials. Silane molecules have zero to three alkoxy groups connected to a central silicon atom and a fourth alkyl chain with varying organofunctional groups such as amine, diamine, methacrylate, epoxy, vinyl, chloro, and phenyl. The alkoxy groups can be converted to silanol groups through hydrolysis reaction by the addition of water separately, from moisture in the air, or from water adsorbed on the surface of nanomaterials. Typically, hydrolysis reactions can be catalyzed by the addition of acids or bases to the reaction medium, whereas several coupling agents, like amine-bearing ones, have shown self-catalysis properties.[11] It is hypothesized that the generated silanol groups can form covalent bonds with hydroxyl groups available on the surface of nanomaterials through a dehydration reaction. Inadvertently, side reactions like homocondensation of the coupling agents may also occur which causes the formation of a highly crosslinked polymer through the formation of Si□O□Si bonds.

H. Riazi, Dr. A. A. Shamsabadi, Prof. M. Soroush
Department of Chemical and Biological Engineering
Drexel University
Philadelphia, PA 19104, USA
E-mail: ms1@drexel.edu
M. Anayee, K. Hantanasirisakul, Dr. B. Anasori, Prof. Y. Gogotsi
A. J. Drexel Nanomaterials Institute and Department of
Material Science and Engineering
Drexel University
Philadelphia, PA 19104, USA
The ORCID identification number(s) for the author(s) of this article can be found under https://doi.org/10.1002/admi.201902008.

DOI: 10.1002/admi.201902008

To date, there have been only a few studies on surface functionalization of MXenes with silane coupling agents.[12–16] Zhang et al. functionalized $Ti_3C_2T_x$ with 3-(methacryloxy) propyltrimethoxysilane (MPS) and subsequently grafted sulfonated polyelectrolyte brushes on the surface by a surface-initiated precipitation polymerization technique.[13] They incorporated the surface functionalized MXene into a poly(ether ether ketone) matrix to fabricate proton conducting membranes. The surface of $Ti_3C_2T_x$ was also functionalized with 1H,1H,2H,2H-perfluorodecyltrimethoxysilane by Zhao et al. and with 1H,1H,2H,2H-perfluorooctyltriethoxysilane by Cao et al. to develop superhydrophobic MXene for solar desalination systems and self-cleaning coatings, respectively.[14,16] Lim et al. also used alkylsilane coupling agents to increase surface hydrophobicity of $Ti_3C_2T_x$ to make it dispersible in nonpolar solvents like hexane.[15] Therefore, silane coupling agents with various organofunctional groups enable a wide variety of applications.

With respect to silane coupling agents possessing amine functional groups, Hao et al. used (3-aminopropyl)triethoxysilane (APTES) to functionalize the surface of $Ti_3C_2T_x$ for thin-film membranes in polyacrylonitrile (PAN) or polydimethylsiloxane (PDMS) matrix, which showed strong enhancement in flux and selectivity for alcohol based solvents.[17] Kumar et al. also used APTES to functionalize the surface of $Ti_3C_2T_x$ for detection of cancer biomarkers.[12] Furthermore, amine functional groups can improve MXene stability and enable MXenes to undergo various reactions such as epoxide ring opening, ureidation, and salt formation with sulfonic and carboxylic acids.[18,19] The previous studies found MXene–aminosilane nanocomposites to be promising potential candidates for various applications. However, none of them investigated the different types of interactions that exist between the silane coupling agents and MXene, the effects of the interactions on the surface charge at different pH values, or thermal decomposition behavior of the functionalized MXenes. Furthermore, as surface functionalization of MXenes should be conducted under mild acidic conditions and inert gas bubbling, to prevent MXene oxidation,[6,20] there is a need for developing a reliable protocol for the functionalization.

To the best of our knowledge, so far only two studies have been published on functionalized MXenes with a positive surface charge. One altered the surface charge using a metal ion and the other using an aminosilane coupling agent.[19,21] However, these studies did not investigate: 1) how surface charge varies with the suspension pH; 2) where the isoelectric point is located, which is important in the layer-by-layer film assembly process; 3) the effect of aminosilane functionalization on thermal behavior of the MXene flakes; 4) the effect of thermal annealing on the interlayer distance of the functionalized MXene flakes; and 5) the chemistry of amine groups after their placement on the MXene surface.

We grafted 3-(2-aminoethylamino)propyltrimethoxysilane (AEAPTMS) on the surface of $Ti_3C_2T_x$. Proton nuclear magnetic resonance (^{1}H NMR) spectroscopy was carried out to confirm the hydrolysis of the AEAPTMS. Fourier-transform infrared spectroscopy (FTIR) was used to confirm the reaction of $Ti_3C_2T_x$ surface hydroxyl groups. X-ray photoelectron spectroscopy (XPS) was utilized to verify the presence of different functional groups on the MXene surface and distinguish the different modes of interactions. Energy-dispersive X-ray spectroscopy (EDS) was performed to confirm the homogenous distribution of AEAPTMS over the surface. Thermogravimetric analysis (TGA) and evolved gas mass spectroscopy (MS) were used to investigate the strength of the interactions between AEAPTMS and $Ti_3C_2T_x$ and confirm that both physically adsorbed and covalently bonded AEAPTMS are available on the surface. Zeta-potential measurements were performed in a wide pH range to confirm the change in the surface charge from negative to positive upon the surface functionalization and find the isoelectric point of the functionalized MXene. Scanning electron microscopy (SEM) and transmission electron microscopy (TEM) were carried out to evaluate the morphology of MXene flakes before and after the surface functionalization. Furthermore, X-ray diffraction (XRD) results showed that the surface functionalization increases the inter-layer distance between the MXene flakes. Finally, to demonstrate applicability of the functionalized MXene, self-assembled MXene films were prepared by mixing the negatively and positively charged $Ti_3C_2T_x$ flakes.

2. Results and Discussion

The chemical reaction between AEAPTMS and the hydroxyl groups of $Ti_3C_2T_x$ is shown schematically in **Figure 1**. Our characterization results indicate that AEAPTMS molecules interact with $Ti_3C_2T_x$ through two modes; the silanol group ends leading to covalent bonding and the amine group ends leading to electrostatic interaction.

Although some primary or secondary amines in the presence of water are able to catalyze the detachment of already

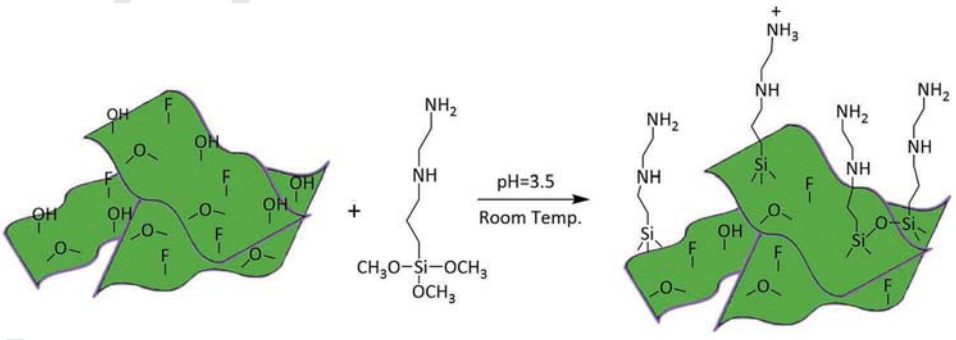

Figure 1. Schematic representation of the pristine $Ti_3C_2T_x$ flakes reacting with the 3-(2-aminoethylamino) propyltrimethoxysilane coupling agent.

bonded coupling agents from the surface of nanomaterials, it has been shown that AEAPTMS does not suffer from this problem in aqueous media.[22] In addition, the chance of a reaction between hydrolyzed methoxy groups of AEAPTMS and hydroxyl groups on the surface of $Ti_3C_2T_x$ is higher for this aminosilane coupling agent compared with its counterparts.[22] In addition to the kind of aminosilane, proper reaction conditions are needed for the completion of the chemical reaction (high grafting efficiency), as discussed below.

The temperature, pH, and water/ethanol ratio are important parameters that dictate the efficacy of the surface functionalization reaction. The parameters were chosen based on the recommended values.[23,24] A reaction medium pH of 3.5 was found to ensure a high grafting efficiency and prevent silane coupling agents from homocondensation.[25,26] The reaction was carried out at room temperature, as dissolved oxygen in water may accelerate $Ti_3C_2T_x$ degradation at higher temperatures.[6] A low ratio of water to ethanol (10/90 wt%) was used to prevent the detachment of the bonded molecules from the surface of $Ti_3C_2T_x$ after functionalization. In fact, water is only needed to convert the methoxy groups of the silane coupling agent to hydroxyl groups through the hydrolysis reaction.[27]

Hydrolysis of AEAPTMS releases methoxy groups in the form of methanol as the reaction side product. Hydrogen bonds between the silanol groups and the –OH surface termination groups of $Ti_3C_2T_x$ are then formed, followed by the formation of covalent bonds between $Ti_3C_2T_x$ and hydrolyzed AEAPTMS (Figure S1C, Supporting Information). In addition, electrostatic attractions between negatively charged surface of $Ti_3C_2T_x$ and the positively charged protonated amine groups of the silane coupling agent may exist. In this case, nonhydrolyzed/hydrolyzed methoxy groups are left nonbonded to the surface (Figure S1A,B, Supporting Information).

We performed ^{1}H NMR spectroscopy to confirm the successful hydrolysis of AEAPTMS. The spectra of AEAPTMS in D_2O as well as a mixture of pristine $Ti_3C_2T_x$ and AEAPTMS in D_2O, in both neutral and acidic media, are presented in **Figure 2**. Regarding ^{1}H NMR results of AEAPTMS, we expected to see eight different peaks as the molecule has eight different kinds of hydrogen (Figure S2, Supporting Information). However, the number of peaks is lower than what is expected (Figure 2A). This may be due to overlapping of some peaks with each other, the hydrogen bonding between the species in the system or other solvent effects.[28–31] Figure 2A shows a sharp peak around 3.3 ppm, which can be attributed to the hydrogens in the methoxy groups (3.3–3.6 ppm).[32] These are the hydrogen that are labeled as type 1 in Figure S2 (Supporting Information). Other small peaks highlighted by vertical arrows I, II, and III in Figure 2A possibly represent other kinds of hydrogens in the silane coupling agent as the system just consists of AEAPTMS, D_2O, and the solvent residue.[32,33] The hydrogens corresponding to each of these arrows are discussed

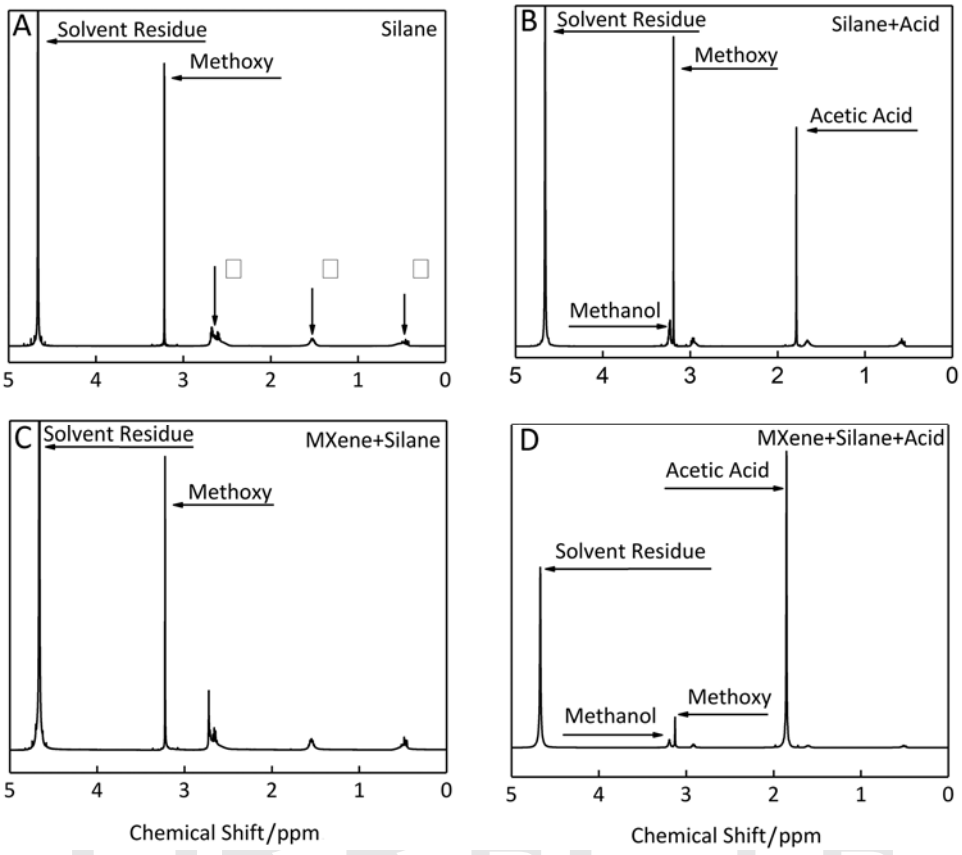

Figure 2. ^{1}H NMR spectra of the silane coupling agent in A) neutral and B) acidic media, and a mixture of MXene/silane coupling agent in C) neutral and D) acidic media.

in Figure S2 (Supporting Information). When acetic acid was added to this system (Figure 2B), a new peak at 3.34 ppm appeared, which verifies the hydrolysis of the methoxy groups and the release of methanol as the side product.[33] The same phenomenon was observed when the silane coupling agent was mixed with pristine $Ti_3C_2T_x$ and the MXene-acetic acid systems (Figure 2C,D). These results show that the presence of $Ti_3C_2T_x$ does not negatively interfere in the hydrolysis reaction. As methoxy groups participated in the hydrolysis reaction, we then expect that the surface functionalization can proceed by a covalent bond formation between the surface of $Ti_3C_2T_x$ and AEAPTMS.

FTIR spectroscopy on the pristine and AEAPTMS-$Ti_3C_2T_x$ (**Figure 3**A) revealed two new peaks at 2924 and 2855 cm^{-1} (inset) that appeared after $Ti_3C_2T_x$ surface functionalization, which are attributed to symmetric and asymmetric vibrations of the C□H bonds in the alkyl chain of AEAPTMS, respectively. Moreover, the peak highlighted by an arrow around 1580 cm^{-1} can be ascribed to the bending mode of N□H bond of the primary amine.[34,35] The broad peak around 3500 cm^{-1} can originate from both surface -OH terminations as well as possibly entrapped water molecules. Thus, the disappearance of this peak in the FTIR spectrum of AEAPTMS-$Ti_3C_2T_x$ can be an indication of successful functionalization of $Ti_3C_2T_x$ with AEAPTMS through the reaction of –OH MXene surface termination groups with silanol groups of AEAPTMS, which results in the conversion of Ti□O□H into Ti□O□Si bonds.[15] Another possibility is that incorporation of large organic molecules on the surface breaks the network of hydrogen bonding between nearby hydroxyl groups which is the cause of broad hydroxyl group peak in FTIR spectra.[36]

To confirm the presence and protonation state of amine groups on the surface of the AEAPTMS-$Ti_3C_2T_x$, the N 1s high resolution XPS spectrum was obtained (Figure 3B, and Tables S1 and S2, Supporting Information). The spectrum was deconvoluted into two peaks corresponding to free and protonated amines at binding energies of 400.2 and 402.0 eV, respectively.[37–39] The ratio of free to protonated amines was found to be ≈1.72:1 based on the ratio of the Relative Sensitive Factor (RSF) adjusted integral area of the two deconvoluted N 1s region peaks. Furthermore, the small peak at ≈397.2 eV is attributed to nitrogen coordinated with a metal which in this case is Ti, thereby forming Ti□N covalent bonds.[40] Similar to the condensation reaction between the silanol groups and the hydroxyl surface terminations forming Ti□O□Si bonds, condensation reaction between the amine groups and the hydroxyl surface terminations leads to release of water and formation of Ti□N bonding. Such Ti□N bonding and condensation reaction have been reported in $Ti_3C_2T_x$ MXene coated on (3-aminopropyl)triethoxy silane modified PET by Park et al.[41] However, due to the low concentration of this specie and thereby low intensity and signal-to-noise ratio, it was not included in the XPS deconvolution analysis. The Si 2p high resolution spectrum (Figure S3, Supporting Information) was fit with a single peak at 102.7 eV corresponding to Si–O–Si linkages between neighboring AEAPTMS molecules arising from polycondensation reactions.[42] Moreover, this same peak can also be attributed to Si–O–Ti linkages which are presumed to exist due to the disappearance of the hydroxyl stretching mode from FTIR and the observance of two types of nitrogen functional groups in the N 1s XPS spectrum which likely originate from the two possible orientations of the AEAPTMS on the surface of $Ti_3C_2T_x$.

Scanning electron microscopy (SEM) is used widely to observe the sheet-like structure of MXenes.[2,43] Here, we conducted SEM on the cross-section of AEAPTMS-$Ti_3C_2T_x$ and found that the layered structure of the pristine MXene stays intact even after functionalization reaction. TEM results also confirmed that MXene keeps its layered structure after the surface functionalization (Figure S4, Supporting Information). We also performed EDS to map the distributions of titanium, fluorine, oxygen, carbon, silicon, and nitrogen in the AEAPTMS-$Ti_3C_2T_x$ structure and its surface (Figure S5, Supporting Information). The first four elements are inherently available in the structure of $Ti_3C_2T_x$, while the presence of silicon and nitrogen atoms are indicative of the surface functionalization (Figure S6, Supporting Information). The nitrogen and silicon are likely to originate from the covalently bonded or the physically adsorbed AEAPTMS molecules as washing process with ethanol was repeated three times after the reaction to remove unreacted silane coupling agents.[44] The results show that the AEAPTMS molecules uniformly distribute on the MXene surface.

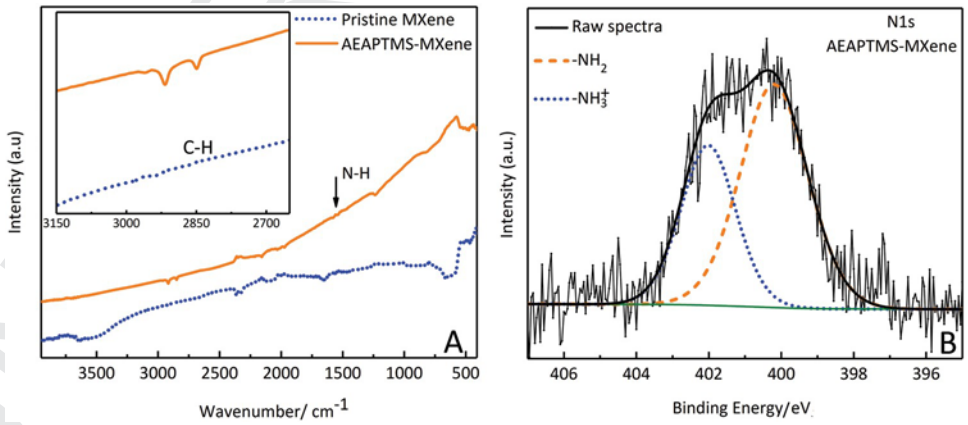

Figure 3. A) FTIR spectra of the pristine $Ti_3C_2T_x$ and the AEAPTMS-$Ti_3C_2T_x$. B) High-resolution N 1s XPS spectrum deconvoluted into two peaks for free (400.2 eV) and protonated amines (402.0 eV).

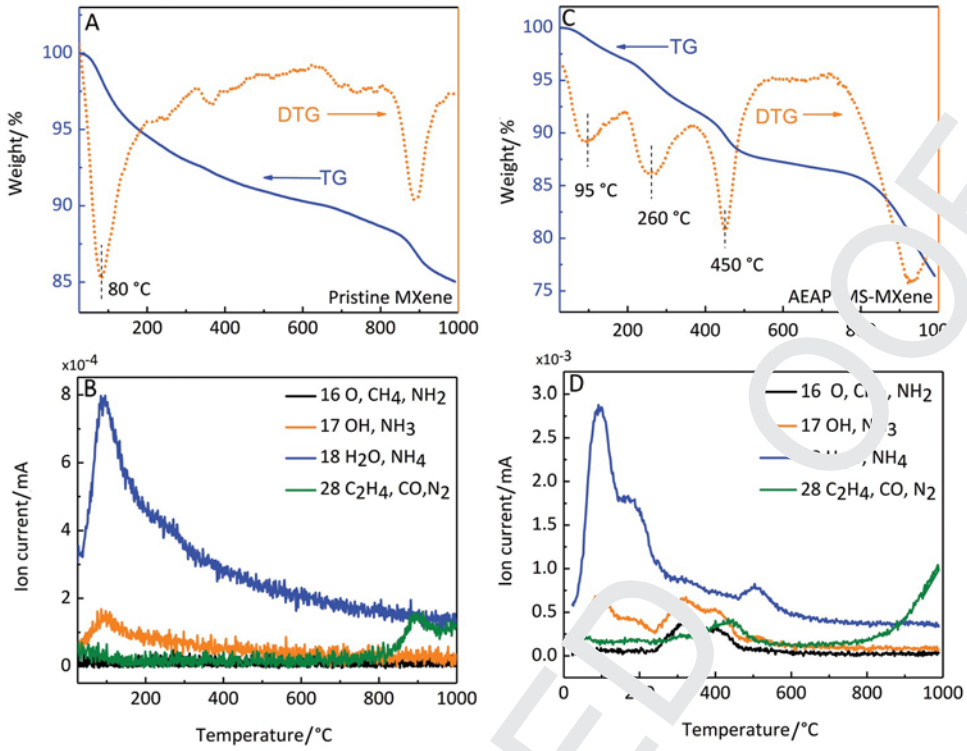

Figure 4. A) TGA thermogram of pristine $Ti_3C_2T_x$ showing one sharp weight loss peak at 25–500 °C; B) mass spectroscopy of pristine $Ti_3C_2T_x$ showing release of H_2O, OH, and CO; C) TGA thermogram of AEAPTMS-$Ti_3C_2T_x$ showing three different weight loss steps in the 25–500 °C range; and D) mass spectroscopy of AEAPTMS-$Ti_3C_2T_x$ showing the release of O, NH_2, OH, H_2O, and CO.

To evaluate the different types and strength of bonding between AEAPTMS and $Ti_3C_2T_x$, TGA and MS of pristine and AEAPTMS-$Ti_3C_2T_x$ were performed and presented in **Figure 4**. The thermogram of pristine MXene indicates the dehydration of the material from 25 °C up to ≈300 °C,[43] which correlates to water ($m/z = 18$) curve in the MS shown in Figure 4B. High temperatures are required to dehydrate free-standing MXene films due to the intercalation of water in small interlayer spacing of ≈10 Å. Decomposition of pristine $Ti_3C_2T_x$ starts ≈750 °C, resulting in CO release as shown by the $m/z = 28$ curve in the Figure 4B.[45,46] Decomposition of $Ti_3C_2T_x$ also results in the evolution of CO_2 and HF gases along with the transformation of the scaffold into titanium carbide (TiC).[47] The AEAPTMS-$Ti_3C_2T_x$ decomposes at the same temperature regime indicating that the decomposition behavior of $Ti_3C_2T_x$ scaffold is not affected by the silane functionalization process.

In contrast, thermogram of the AEAPTMS-$Ti_3C_2T_x$ exhibits three distinct weight loss steps in the 25–500 °C range. The first step with a maximum rate of change at ≈95 °C corresponds to the desorption of water and ethanol from AEAPTMS-$Ti_3C_2T_x$. The shoulder at ≈175 °C in the ($m/z = 18$ and 17) spectra can be attributed to the dehydration of the intercalated water molecules. The boiling point of pure AEAPTMS is ≈260 °C which corresponds well with the second TGA weight loss step having a maximum rate of change at ≈260 °C.[48] The sharp increase in the methane and amine anion ($m/z = 16$) and ammonia ($m/z = 17$) release starting at ≈240 °C with a maximum at ≈315 °C agree well with the evolution of physiosorbed AEAPTMS. The slight increase in this temperature from 260 to 315 °C can also be ascribed to the intercalation of the AEAPTMS in the interlayer spacing of $Ti_3C_2T_x$ and to electrostatic interactions between NH_3^+ of AEAPTMS and –OH surface termination groups of the $Ti_3C_2T_x$. The third weight loss step in the thermogram can be related to the loss of AEAPTMS covalently bonded to $Ti_3C_2T_x$ as indicated by the onset and maximum in the derivative thermogravimetry (DTG) curve at ≈350 °C and ≈450 °C, respectively. Moreover, the peaks in the methane, amine ($m/z = 16$) and ammonia ($m/z = 17$) MS curves at ≈400 °C and the peak in the CO ($m/z = 28$) MS curve at ≈438 °C further corroborate the decomposition of covalently bonded AEAPTMS.

Overall, the TGA results here are consistent with reports on GLYMO-TiO_2,[49] APTES-SiO_2,[50] and other surface functionalized nanoparticles,[51,52] in which three weight loss steps exist in the 25–500 °C range. Yamazaki et al. attributed the three weight loss steps to physiosorbed monomeric silanes, physiosorbed polycondensated silanes, and chemisorbed silanes.[50] Salon et al. indicated that compared to silane coupling agents with other functional groups, those based on amino groups exhibit fast polycondensation kinetics, hence the expected large second weight loss step.[53] Overall, the exact control of each of those types of interactions is out of the scope of this research; However, the presence of chemisorbed silane species on the $Ti_3C_2T_x$ surface expands the applications of this functionalized MXene.

Another indication of the presence of free amine groups on AEAPTMS-$Ti_3C_2T_x$ surface is the change in its surface charge. Zeta potential measurements were conducted on the pristine and functionalized MXene dispersions in a pH range of ≈2.5 to ≈12, within pristine $Ti_3C_2T_x$ MXene colloid is stable.

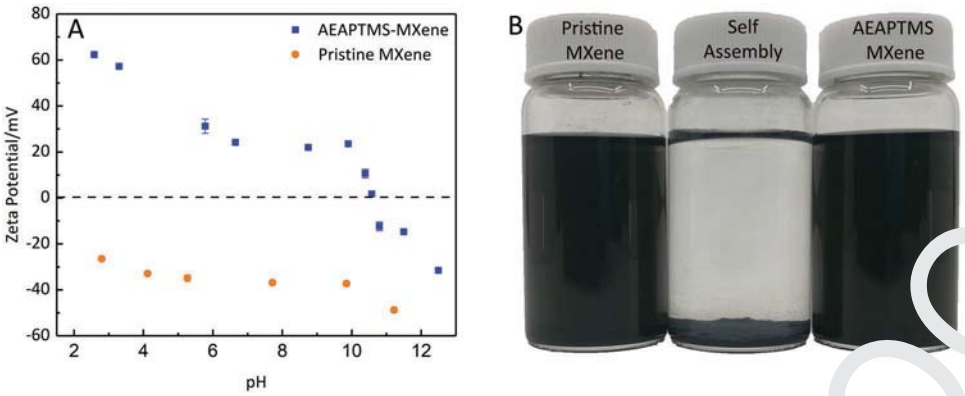

Figure 5. A) Surface charge of the pristine MXene and AEAPTMS-$Ti_3C_2T_x$ versus pH, and B) self-assembled film obtained from mixing the positively charged functionalized MXene and the negatively charged pristine MXene.

$Ti_3C_2T_x$ MXene in strongly basic medium (pH > 12) degrades quickly due to attack by hydroxyl ions. On the other hand, $Ti_3C_2T_x$ MXene dispersions in strongly acidic medium (pH < 2.5) agglomerate and settle out of solution due to high concentration of H^+ ion, which leads to self-assembly and structuring of the sheets.[54] Unlike pristine $Ti_3C_2T_x$ which has a negative surface charge in the pH range of ≈2.5 to ≈12, AEAPTMS-$Ti_3C_2T_x$ showed a positive surface charge of more than 20 mV in a wide pH window from ≈2.5 to ≈10 enabling it to participate in further surface functionalization reactions in neutral media (**Figure 5**A). The AEAPTMS-$Ti_3C_2T_x$ also keeps its pH responsiveness as free amine groups, similar to hydroxyl groups, are capable of gaining or losing H^+ upon change in the medium pH.[34] As the pH increases, the concentration of H^+ ions decreases and the concentration of OH^- ions increases, leading to deprotonation of the ammonium group and a decrease in the overall positive charge of the particle. Likewise, as the pH decreases, protonation of the amine group occurs which increases the overall positive charge of the particle.[55–57] The AEAPTMS-$Ti_3C_2T_x$ has an isoelectric point between pH 10.58 and 10.8 as indicated by the surface charges of +1.73 and −12.34 mV, respectively. Furthermore, the surface charge of +62 mV at pH = 2.58 is the largest positive charge reported for MXenes to date.

From the application point of view, the synthesis of a positively charged $Ti_3C_2T_x$ allows for its self-assembly with the pristine MXene, which inherently possesses a negative surface charge.[58] Figure 5B represents the pristine MXene, AEAPTMS-$Ti_3C_2T_x$, and the layer obtained from their assembly. Xie et al. used layer-by-layer assembled films made from positively charged carbon nanotubes and pristine MXene to fabricate electrodes for sodium-based batteries.[59] In their research, the carbon nanotube acted as a spacer between MXene sheets. Here, similarly, electrostatic interactions make it possible to form a film while the restacking of the MXene nanosheets can be prohibited due to the grafted aminosilane molecules, which potentially play the role of a spacer.

XRD measurements on free-standing pristine and functionalized $Ti_3C_2T_x$ films both annealed at 250 °C showed an increase in the interlayer spacing from 11.7 to 13.2 Å upon surface functionalization based on shift of the (002) peak from 7.55° to 6.67° (Figure S7, Supporting Information). Similarly, for the samples at room temperature and the ones annealed at 60 °C, functionalized MXene showed a peak at lower angles (larger interlayer spacing) compared with the corresponding pristine MXene. Furthermore, the broadening of the (002) peak after functionalization and heat treatment at 250 °C is due to less regular spacing between the layers after removal of intercalated solvent and physically adsorbed aminosilane, which leave behind only chemically bonded silanes. The increase in the interlayer spacing can still be seen through the tail toward lower 2θ values.

Overall, the presence of free amine groups on the surface of AEAPTMS-$Ti_3C_2T_x$ that are available for subsequent reactions opens the door for a wide variety of applications. For example, functionalized MXenes can act as curing agents for epoxy resins and allow the development of electrically conductive composites.[60] In addition, they can play the role of substrates for surface-initiated atom transfer radical polymerization, electrodes for energy-storage devices and metal ion absorber.[61–64] The results presented in this article point to the potential of MXenes for self-assembly, which permits bottom-up manufacturing of nanodevices. Ensembles of nanoparticles made by self-assembly are used in nanoscale thermometer, data storage devices, catalysis recovery, magnetic data storage, delivery of biologically active species, electrochemical biosensors, etc.[65]

3. Conclusion

The surface of $Ti_3C_2T_x$ was functionalized with AEAPTMS. Hydroxyl groups on the surface of the pristine $Ti_3C_2T_x$ provide suitable sites for the aminosilane grafting. By doing so, we were able to change the surface charge of $Ti_3C_2T_x$ from highly negative to +62 mV at pH = 2.58, which is the largest positive zeta potential value reported for MXenes. Our results showed that the AEAPTMS-$Ti_3C_2T_x$ is still a pH responsive nanomaterial due to the presence of amine groups on its surface, which are capable of adsorbing or desorbing protons upon change in pH. The simultaneous presence of protonated and free amine groups on the surface of AEAPTMS-$Ti_3C_2T_x$ was confirmed by XPS. Homogenous distributions of silicon and nitrogen elements were also observed by EDS. All characterization results together confirmed the presence of amine groups

on the surface of the AEAPTMS-$Ti_3C_2T_x$. This functionalization method should be applicable to other MXene structures and compositions. The amine functionalization expands the range of applications of MXenes in many areas such as antibacterial coatings, fuel cells, surface-initiated polymerization, dye adsorbents, and drug delivery systems.

4. Experimental Section

Materials: Ethanol (anhydrous ≥99.9%) was purchased from Electron Microscopy Science Co. Sodium hydroxide (NaOH) (≥97%) was purchased from Merck Co., and glacial acetic acid (CH_3COOH) (100%) was supplied by BDH Co. AEAPTMS (≥96%) and deuterium oxide (D_2O) with 99.8% atom D were purchased from Alfa Aesar. Hydrochloric acid (HCl) (41–58%), and lithium fluoride (LiF) (99.98%) were purchased from Fisher Scientific Co. Ti_3AlC_2 was obtained from Carbon Ukraine (Kyiv, Ukraine). The polypropylene membrane, 3501 Coated PP, was purchased from Celgard LLC Co. (Charlotte, NC, US). All chemicals were used as they were received (without any purification).

$Ti_3C_2T_x$ MXene Synthesis: Ti_3AlC_2 MAX phase was selectively etched to form $Ti_3C_2T_x$ by adding Ti_3AlC_2 (2 g, <75 μm particle size) to an etchant solution containing LiF (3.2 g) and HCl (9 M, 40 mL) over the course of ≈5 min to avoid overheating due to the exothermic nature of the reaction. The suspension was stirred at 300 rpm with a polytetrafluoroethylene (PTFE) coated stir bar at room temperature for 24 h in a loosely capped polyethylene terephthalate (PET) bottle. The resulting suspension was washed five times via centrifugation at 3500 rpm for 5 min with DI water in a 175 mL centrifuge tube until the pH reached ≈6. Following washing, the suspension was bath-sonicated for 1 h at 100 W using a bath sonicator (2510 Branson). Next, the suspension was centrifuged at 3500 rpm for 5 min to remove multilayer MXene and unetched MAX. The supernatant was then centrifuged at 10 000 rpm for 2 h to concentrate the solution.

$Ti_3C_2T_x$ Functionalization Procedure: Surface functionalization of $Ti_3C_2T_x$ was carried out in a water/ethanol mixture (10/90 wt%) in order to provide enough amount of water for AEAPTMS hydrolysis reaction. The reaction was performed at room temperature and its medium was stirred (600 rpm) for 8 h under nitrogen bubbling. First, ethanol was added to an aqueous suspension of $Ti_3C_2T_x$, and acetic acid was then added to decrease the pH of the reaction medium to 3.5. To obtain the concentration of $Ti_3C_2T_x$ suspensions, a given volume of each suspension was first vacuum filtered and the mass of the corresponding freestanding film was then measured. A part of the total ethanol used for the reaction, was reserved for preparing silane in ethanol solution. To ensure the occurrence of the reaction between OH terminations of $Ti_3C_2T_x$ and AEAPTMS, a silane to $Ti_3C_2T_x$ mass ratio of 2:1 was used. Next, the solution of the silane coupling agent in ethanol was added dropwise to the reaction medium during the first 2 h of the reaction. After completion of the reaction, the suspension was washed three times with ethanol by centrifugation at 3500 rpm to remove unreacted silane coupling agents from AEAPTMS-$Ti_3C_2T_x$ nanosheets. The final suspension was vacuum-filtered on polypropylene membranes and the obtained free-standing films were subsequently dried in vacuum oven at 60 °C for 24 h. To get $Ti_3C_2T_x$ powder, the final suspension was cast in a Teflon petri dish and kept under vacuum to evaporate its liquid medium.

Characterization: Fourier-transform infrared (FTIR) spectroscopy on pristine and AEAPTMS-$Ti_3C_2T_x$ powders (Thermo Fisher Nicolet iS50 FTIR Spectrometer, USA) was carried out in attenuated total reflectance (ATR) mode with a diamond crystal in the range of 4000–400 cm^{-1} with a step size of 0.5 cm^{-1} and 32 measurement cycles.

Zeta potential measurements (NanoBrook ZetaPALS, Brookhaven Instrument, USA) were performed on the AEAPTMS-$Ti_3C_2T_x$ powder redispersed in water by sonication for 30 min as well as on the pristine MXene. NaOH and CH_3COOH aqueous solutions were used to adjust the pH of the system. Each test was repeated at least three times and the average values along with their uncertainty range were reported.

Thermogravimetric analysis and evolved gas mass spectrometry were carried out on the pristine MXene and AEAPTMS-$Ti_3C_2T_x$ free-standing films using SDT 650 TGA coupled with Discovery MS (TA Instruments, USA). The tests were conducted from room temperature to 1000 °C with a heating rate of 10 °C min^{-1} under a flowing helium atmosphere at 100 mL min^{-1}. Prior to the test, the furnace was purged with 100 mL min^{-1} of helium for 1 h to remove residual air.

X-ray photoelectron spectroscopy (XPS) was conducted on the free-standing fi using PHI VersaProbe 5000 instrument (Physical Electronics, USA) with a 200 μm and 50 W monochromatic Al Kα (1486.6 eV) X-ray source. Charge neutralization was accomplished through a dual beam setup using low energy Ar^+ ions and low energy electrons at 1 eV/200 μA. High-resolution F 1s, O 1s, Ti 2p, N 1s, C 1s, Si 2p, and Fermi energy region spectra were collected using a pass energy of 23.5 eV and an energy resolution of 0.05 eV. Survey spectrum was collected using a pass energy of 117 eV and an energy resolution of 0.5 eV. No binding energy scale correction was applied as the samples were not charged during the analysis. Quantifi and peak fi were conducted using CasaXPS V2.3.19.

^1H NMR spectroscopy (500 MHz Varian Unity Inova NMR, USA) was performed by dissolving AEAPTMS in D_2O or dispersing a mixture of $Ti_3C_2T_x$ powder and AEAPTMS in D_2O. The suspension of $Ti_3C_2T_x$ in D_2O was prepared by bath-sonication (Branson 1200) for 30 min to ensure fine dispersion of the nanomaterial in D_2O. pH of the system was adjusted by adding CH_3COOH.

Scanning electron microscopy (SEM) and energy-dispersive X-ray spectroscopy (EDS) were carried out, respectively, using Zeiss Supra 50 VP, USA, and an EDS detector (Oxford Instruments, Ultim Max) mounted on it. Samples were prepared by drop-casting of the AEAPTMS-$Ti_3C_2T_x$ suspension on a microscope glass to obtain powdered material. The samples were then mounted on carbon tape and sputter-coated with platinum.

Transmission electron microscopy (TEM) was carried out using a JEOL JEM2100 microscope. Samples were prepared by drop-casting of the pristine $Ti_3C_2T_x$ and AEAPTMS-$Ti_3C_2T_x$ suspensions on TEM grids. The girds were then placed in a desiccator connected to a vacuum pump to assure that the samples were dried completely.

X-ray diffraction (XRD) (Rigaku Miniflex 600 diffractometer) was conducted on free-standing films using a monochromatic Cu Kα X-ray source. Survey scans were conducted from 3° to 65° with a step size of 0.03° at 5° min^{-1}. High-resolution scans were conducted from 3° to 10° with a step size of 0.01° at 0.5° min^{-1}.

Supporting Information

Supporting Information is available from the Wiley Online Library or from the author.

Acknowledgements

H. Riazi and A. A. Shamsabadi were partially supported by the U.S. National Science Foundation under Grant No. CBET-1804285. Any opinions, findings, and conclusions or recommendations expressed in this material are those of the authors and do not necessarily reflect the views of the National Science Foundation.

Conflict of Interest

The authors declare no conflict of interest.

Keywords

aminosilane, MXene, self-assembly, surface functionalization, $Ti_3C_2T_x$

Received: November 28, 2019
Published online:

[1] B. Anasori, Y. Gogotsi, *2D Metal Carbides and Nitrides (MXenes)*, Springer, Berlin **2019**.
[2] B. Anasori, M. R. Lukatskaya, Y. Gogotsi, *Nat. Rev. Mater.* **2017**, *2*, 16098.
[3] A. A. Shamsabadi, M. Gh, B. Anasori, M. Soroush, *ACS Sustainable Chem. Eng.* **2018**, *6*, 16586.
[4] M. Naguib, V. N. Mochalin, M. W. Barsoum, Y. Gogotsi, *Adv. Mater.* **2014**, *26*, 992.
[5] M. Malaki, A. Maleki, R. S. Varma, *J. Mater. Chem. A* **2019**, *7*, 10843.
[6] C. J. Zhang, S. Pinilla, N. McEvoy, C. P. Cullen, B. Anasori, E. Long, S.-H. Park, A. s. Seral-Ascaso, A. Shmeliov, D. Krishnan, *Chem. Mater.* **2017**, *29*, 4848.
[7] C. E. Ren, K. B. Hatzell, M. Alhabeb, Z. Ling, K. A. Mahmoud, Y. Gogotsi, *J. Phys. Chem. Lett.* **2015**, *6*, 4026.
[8] M. Naguib, R. R. Unocic, B. L. Armstrong, J. Nanda, *Dalton Trans.* **2015**, *44*, 9353.
[9] Z. Zhou, J. Liu, X. Zhang, D. Tian, Z. Zhan, C. Lu, *Adv. Mater. Interfaces* **2019**, *6*, 1802040.
[10] M. Lu, W. Han, H. Li, H. Li, B. Zhang, W. Zhang, W. Zheng, *Adv. Mater. Interfaces* **2019**, *6*, 1900160.
[11] M.-C. B. Salon, M. Abdelmouleh, S. Boufi, M. N. Belgacem, A. Gandini, *J. Colloid Interface Sci.* **2005**, *289*, 249.
[12] S. Kumar, Y. Lei, N. H. Alshareef, M. Quevedo-Lopez, K. N. Salama, *Biosens. Bioelectron.* **2018**, *121*, 243.
[13] J. Zhang, Y. Liu, Z. Lv, T. Zhao, P. Li, Y. Sun, J. Wang, *Solid State Ionics* **2017**, *310*, 100.
[14] J. Zhao, Y. Yang, C. Yang, Y. Tian, Y. Han, J. Liu, X. Yin, W. Que, *J. Mater. Chem. A* **2018**, *6*, 16196.
[15] S. Lim, H. Park, J. Yang, C. Kwak, J. Lee, *Colloids Surf. A* **2019**, *579*, 123648.
[16] W.-T. Cao, W. Feng, Y.-Y. Jiang, C. Ma, Z.-F. Zhou, M.-G. Ma, Y. Chen, F. Chen, *Mater. Horiz.* **2019**, *6*, 1057.
[17] L. Hao, H. Zhang, X. Wu, J. Zhang, J. Wang, Y. Li, *Composites, Part A* **2017**, *100*, 139.
[18] E. P. Plueddemann, *Silane Coupling Agents*, Springer Science+Business Media, LLC, New York **1991**.
[19] J. Ji, L. Zhao, Y. Shen, S. Liu, Y. Zhang, *FlatChem* **2019**, *17*, 100128.
[20] S. Seyedin, E. R. S. Yanza, J. M. Razal, *J. Mater. Chem. A* **2017**, *5*, 24076.
[21] Z. Huang, L. Biwu, L. Juewen, *Langmuir* **2019**, *35*, 9858.
[22] M. Zhu, M. Z. Lerum, W. Chen, *Langmuir* **2012**, *28*, 416.
[23] M.-C. B. Salon, M. N. Belgacem, *Colloids Surf. A* **2010**, *366*, 147.
[24] O. Paquet, M.-C. B. Salon, E. Zeno, M. N. Belgacem, *Mater. Sci. Eng., C* **2012**, *32*, 487.
[25] R. Bel-Hassen, S. Boufi, M.-C. B. Salon, M. Abdelmouleh, M. N. Belgacem, *J. Appl. Polym. Sci.* **2008**, *108*, 1958.
[26] H. Ishida, J. L. Koenig, *J. Colloid Interface Sci.* **1978**, *64*, 555.
[27] X. Liu, J. Xing, Y. Guan, G. Shan, H. Liu, *Colloids Surf. A* **2004**, *238*, 127.
[28] Y. Tataurova, M. J. Sealy, R. G. Larsen, S. C. Larsen, *J. Phys. Chem. Lett.* **2012**, *3*, 425.
[29] L. Yao, A. Grishaev, G. Cornilescu, A. Bax, *J. Am. Chem. Soc.* **2010**, *132*, 10866.
[30] J. W. Akitt, B. E. Mann, *NMR and Chemistry: An Introduction to Modern NMR Spectroscopy*, CRC Press, Boca Raton, FL **2000**.
[31] P. Needham, *Stud. Hist. Philos. Sci., Part A* **2013**, *44*, 51.
[32] S. Sasaki, *Handbook of Proton-NMR Spectra and Data*, Academic Press, New York **1985**.
[33] G. R. Fulmer, A. J. Miller, N. H. Sherden, H. E. Gottlieb, A. Nudelman, B. M. Stoltz, J. E. Bercaw, K. I. Goldberg, *Organometallics* **2010**, *29*, 2176.
[34] J. Zhao, M. Milanova, M. M. Warmoeskerken, V. Dutschk, *Colloids Surf. A* **2012**, *413*, 273.
[35] X. Wang, W. Xing, P. Zhang, L. Song, H. Yang, Y. Hu, *Compos. Sci. Technol.* **2012**, *72*, 737.
[36] T. Kondo, *Cellulose* **1997**, *4*, 281.
[37] J. Pels, F. Kapteijn, J. Moulijn, Q. Zhu, K. Thomas, *Carbon* **1995**, *33*, 1641.
[38] R. Jansen, H. Van Bekkum, *Carbon* **1995**, *33*, 1021.
[39] R. Liu, W. Li, *ACS Omega* **2018**, *3*, 2609.
[40] D. Jaeger, J. Patscheider, *Surf. Sci. Spectra* **2013**, *20*, 1.
[41] T. H. Park, S. Yu, M. Koo, H. Kim, E. H. Kim, J. E. Park, B. Ok, B. Kim, S. H. Noh, C. Park, E. Kim, C. M. Koo, C. Park, *ACS Nano* **2019**, *13*, 6835.
[42] P. C. Ma, J.-K. Kim, B. Z. Tang, *Carbon* **2006**, *44*, 3232.
[43] J. L. Hart, K. Hantanasirisakul, A. C. Lang, B. Anasori, D. Pinto, Y. Pivak, J. T. van Omme, S. J. May, Y. Gogotsi, M. L. Taheri, *Nat. Commun.* **2019**, *10*, 522.
[44] F. Ahangaran, A. Hassanzadeh, S. Nouri, *Int. Nano Lett.* **2013**, *3*, 23.
[45] J. Zhu, E. Ha, G. Zhao, Y. Zhou, D. Huang, G. Yue, L. Hu, N. Sun, Y. Wang, L. Y. S. Lee, *Coord. Chem. Rev.* **2017**, *352*, 306.
[46] Y. Cao, Q. Deng, Z. Liu, D. Shen, T. Wang, Q. Huang, S. Du, N. Jiang, C.-T. Lin, J. Yu, *RSC Adv.* **2017**, *7*, 20494.
[47] Z. Li, L. Wang, D. Sun, Y. Zhang, B. Liu, Q. Hu, A. Zhou, *Mater. Sci. Eng., B* **2015**, *191*, 33.
[48] M. Ash, *Handbook of Fillers, Extenders, and Diluents*, Synapse Info Resources, Inc., New York **2007**.
[49] W. Que, Y. Zhou, Y. Lam, Y. Chan, C. Kam, *J. Sol–Gel Sci. Technol.* **2001**, *20*, 187.
[50] R. Yamazaki, N. Karyu, M. Noda, S. Fujii, Y. Nakamura, *J. Appl. Polym. Sci.* **2016**, *133*.
[51] A. Shanmugharaj, J. Bae, K. Y. Lee, W. H. Noh, S. H. Lee, S. H. Ryu, *Compos. Sci. Technol.* **2007**, *67*, 1813.
[52] Z. Luan, J. A. Fournier, J. B. Wooten, D. E. Miser, *Microporous Mesoporous Mater.* **2005**, *83*, 150.
[53] M.-C. B. Salon, P.-A. Bayle, M. Abdelmouleh, S. Boufi, M. N. Belgacem, *Colloids Surf. A* **2008**, *312*, 83.
[54] S. J. Kim, J. Choi, K. Maleski, K. Hantanasirisakul, H. T. Jung, Y. Gogotsi, C. W. Ahn, *ACS Appl. Mater. Interfaces* **2019**, *11*, 32320.
[55] L. Liu, Z. Guo, Z. Huang, J. Zhuang, W. Yang, *Sci. Rep.* **2016**, *6*, 22029.
[56] S. H. Huang, D. H. Chen. *J. Hazard. Mater.* **2009**, *163*, 174.
[57] X. He, K. Wang, D. Li, W. Tan, C. He, S. Huang, B. Liu, X. Lin, X. Chen, *J. Dispersion Sci. Technol.* **2003**, *24*, 633.
[58] J. Yang, W. Bao, P. Jaumaux, S. Zhang, C. Wang, G. Wang, *Adv. Mater. Interfaces* **2019**, *6*, 1802004.
[59] X. Xie, M.-Q. Zhao, B. Anasori, K. Maleski, C. E. Ren, J. Li, B. W. Byles, E. Pomerantseva, G. Wang, Y. Gogotsi, *Nano Energy* **2016**, *26*, 513.
[60] S. Wang, Z. Liang, T. Liu, B. Wang, C. Zhang, *Nanotechnology* **2006**, *17*, 1551.
[61] A. VahidMohammadi, J. Moncada, H. Chen, E. Kayali, J. Orangi, C. A. Carrero, M. Beidaghi, *J. Mater. Chem. A* **2018**, *6*, 22123.
[62] A. Ali, K. Hantanasirisakul, A. Abdala, P. Urbankowski, M.-Q. Zhao, B. Anasori, Y. Gogotsi, B. Aïssa, K. A. Mahmoud, *Langmuir* **2018**, *34*, 11325.
[63] S. B. Ambade, R. B. Ambade, W. Eom, S. H. Noh, S. H. Kim, T. H. Han, *Adv. Mater. Interfaces* **2018**, *5*, 1801361.
[64] L. Fu, Z. Yan, Q. Zhao, H. Yang, *Adv. Mater. Interfaces* **2018**, *5*, 1801094.
[65] Z. Nie, A. Petukhova, E. Kumacheva, *Nat. Nanotechnol.* **2010**, *5*, 15.

